Article

Effective Electrons Transfer Pathway of the Ternary TiO_2/RGO/Ag Nanocomposite with Enhanced Photocatalytic Activity under Visible Light

Hongwei Tian [1,*], Chenxing Wan [1], Xin Xue [2], Xiaoying Hu [3] and Xiaoyi Wang [4,*]

[1] Department of Materials Science and Key Laboratory of Automobile Materials of MOE, Jilin University, Changchun, China; 626374440@qq.com
[2] The Second Hospital, Jilin University, Changchun, China; xuexinsir@163.com
[3] College of Science, Changchun University, Changchun, China; huxy@ccu.edu.cn
[4] Key Laboratory of Optical System Advanced Manufacturing Technology, Changchun Institute of Optics, Fine Mechanics and Physics, Chinese Academy of Sciences, Changchun, 130033, China
* Correspondence: tianhw@jlu.edu.cn (H.T.); wangxiaoyi1977@sina.com (X.W.); Tel.:+86-0431-8516-8444(H.T.); +86-0431-8670-8126(X.W.)

Abstract: Mesoporous TiO_2/reduced graphene oxide/Ag (TiO_2/RGO/Ag) ternary nanocomposite with effective electrons transfer pathway is obtained by an electrostatic self-assembly method and photo-assisted treatment. Compared with bare mesoporous TiO_2 (MT) and mesoporous TiO_2/RGO (MTG), the ternary mesoporous TiO_2/RGO/Ag (MTGA) nanocomposite exhibited superior photocatalytic performance for the degradation of MB under visible light, and the degradation rate reached 0.017 min-1, which was 3.4 times higher than that of MTG. It is proposed that Ag nanoparticles can form the local surface plasmon resonance (LSPR) to absorb the visible light and distract the electrons into MT, and RGO can accept the electrons from MT to accelerate the separation efficiency of carriers. The establishment of MTGA ternary nanocomposite make the three components act synergistic effect to enhance the photocatalytic performance.

Keywords: mesoporous TiO_2; reduced graphene oxide; Ag nanoparticles; photocatalytic activity; visible light irradiation

1. Introduction

As a promising wide-bandgap semiconductor material, titanium dioxide (TiO_2) has been widely applied in the field of photocatalysis.[1,2] TiO_2 photocatalyst is acknowledged as the most suitable material due to its excellent adjustable microstructure, chemical stability, non-toxicity, easy practicality and low cost.[3-6] However, there are still some defects mainly concentrating in the high recombination rate of photogenerated carriers and only absorbing UV light. The usual way for overcoming these shortcomings is coupling with sensitizing agents, narrow-bandgap semiconductor, and non-metal-doping or with noble metal materials.[7-13]

Graphene, a promising material with the traits of large surface area, high conductivity, good transparency and high stability, has attracted great recent attention in various fields.[14-16] Combining TiO_2 with graphene could enhance the photocatalytic capacity, which facilitates the charge separation and transportation and suppresses the recombination of photogenerated electrons and holes.[17-19] Besides graphene, the decoration of noble metal Ag could enhance the photocatalytic activity of TiO_2 photocatalysts, due to the LSPR effect for optimizing the use of solar energy and improving the transfer efficiency of photogenerated carriers.[11,20-24]

In recent years, constructing a ternary structure has turned into an effective tactic to enhance the absorbing of solar light and photocatalytic capability. Xian et.al reported that the obtained TiO_2 nanotube array–graphene–CdS quantum dots (TNT-GR-CdS) composite film revealed higher photoelectric response and photocatalytic activities than other bare TNT, TNT-CdS and TNT-GR.[25] Myilsamy et.al synthesized by sol–gel route indium and cerium co-doped mesoporous TiO_2

nanocomposite with shifted the light absorption band-edge position to visible region and the efficiently suppressed electron–hole recombination.[26] Li and his co-workers prepared graphene/Fe^{3+}-doped TiO_2 nanowire composites, it was found that Fe^{3+} doping could keep the more direct contact between TiO_2 and graphene and improved the response of TiO_2 nanowires.[27] To date, more similar ternary structures have appeared in pace with the higher requirement for the photocatalytic capability of materials, e.g., TiO_2/$InVO_4$/RGO[28], C, N co-doping mesoporous Au/TiO_2[29] and Ag-AgBr/TiO_2[30].

Accordingly, combining Ag and graphene with TiO_2 to build the ternary skeleton can enhance the photocatalytic performance of TiO_2 due to the collective effect of Ag nanoparticles and graphene. Shah et al. successfully synthesized by the solvothermal process Ag–TiO_2–reduced graphene oxide ternary nanocomposite, which showed enhanced photocatalytic activity for degradation of rhodamine B dye under visible light irradiation.[23] Vasilaki et.al used chemical reduction to load Ag nanoparticles onto P25 and hydrothermal to get reduced graphene oxide sheets.[31] Liu et.al made use of hydrothermal synthesis to construct 3D urchin-like Ag/TiO_2/reduced graphene oxide composites.[11] Tan et al. designed a series of noble metal (Pt, Pd, Ag and Au) nanoparticles supported on reduced graphene oxide/TiO_2 utilizing the solvothermal process and the polyol to combine RGO and reduce metal ions into metal, respectively. The ternary nanocomposite exhibited enhanced photocatalytic activities toward the photoreduction of CO_2 into CH_4 gas under their radiation of typical day light bulbs.[32] However, in most TiO_2/RGO/Ag ternary systems under visible light, most of reported innovations mainly concentrated in synthesis means, microscopic morphology or application performance. Few reports formally proposed the electron-transfer mechanism that jumping into the conduction band (CB) of TiO_2 from Ag. Herein, we put forward a possible electron transfer pathway that the electrons migrate from Ag nanoparticles to CB of TiO_2, then RGO nanosheets receive electrons from TiO_2 to increase the separation rate of the photogenerated electron-hole pairs.

In this work, we utilized an electrostatic self-assembly approach and a photo-assisted reduction process to complete the decoration of Ag nanoparticles and RGO nanosheets on the basis of mesoporous TiO_2. Compared with MT and MTG, the ternary MTGA nanocomposite exhibited superior photocatalytic performance for the degradation of MB under visible light irradiation, and the degradation rate reached 0.017 min^{-1}, which was 3.4 times of MTG's. More importantly, the enhancement of the photocatalytic activity could be ascribed to the large specific surface area, the extensive photo response regions, and the highly efficient separation and transmission of the photo-induced charge carriers caused by the feasible electron-transfer pathway.

2. Results and Disscussion

Figure 1 depicts the XRD spectra of MT, MTG and MTGA nanocomposites, indicating that the diffraction peaks at 25.3°, 37.8°, 48.0°, 53.9°, 55.1°,62.7°, 70.3° and 75.0° of MT could well match with the (101), (004), (200), (105), (204), (220) and (215) planes of the anatase-phase TiO_2 (JCPDS no. 21-1272). There are no obvious diffraction peaks of RGO in the sample of MTG, duo to the low contents of RGO. After photo-assisted loaded Ag nanoparticles, there are two peaks at 38.1° and 44.2° in accordance with the typical diffraction peaks of Ag (JCPDS no. 04-0783), corresponding to the (111) and (200) planes of Ag nanoparticles. Specifically, the peak of the (111) plane is covered by TiO_2's (004), but the intensity of this peak is heightened by Ag nanoparticles compared with MT and MTG, and the intensity of another peak located at 44.2° is relatively weak because of the low doped and high dispersed of Ag nanoparticles.

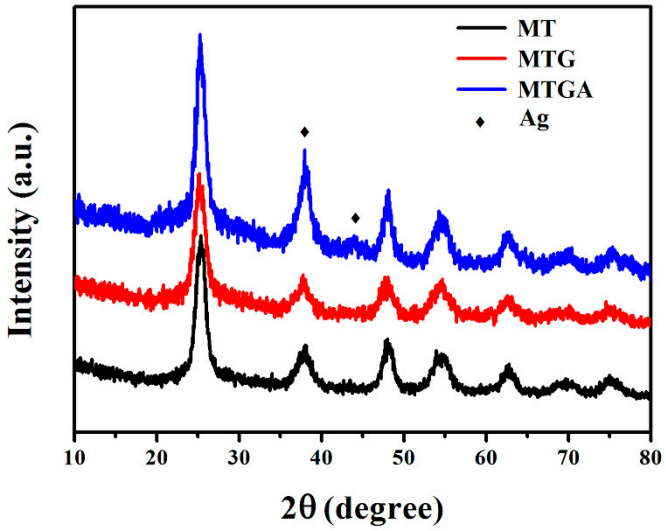

Figure 1. XRD spectra of MT, MTG, MTGA;

The resulting Raman spectra of MT, MTG and MTGA nanocomposites as shown in Figure 2. highlights four particular peaks owing to anatase-phase TiO_2 located at 146 (Eg), 399 (B1g), 517(A1g) and 639 cm^{-1} (Eg) emerge in all of samples.[33] Besides that, the inset of Figure 2. shows the Raman spectrum of GO with two manifest peaks at 1351 cm^{-1} (D-band) and 1605 cm^{-1} (G-band). The D-band originates from the disorder with structural defects caused in the process of the reduction of GO. Meanwhile, the G-band corresponds to the first order scattering of E2g photon of sp2 C atoms of graphene.[19,27] Therefore, the intensity ratio (ID/IG) for GO was 0.88 signifying the existence of plentiful sp3 in the sample. The D and G-bands of MTG and MTGA were approximately in the same position with GO. However, the ID/IG of MTG and MTGA decreased to 0.69 and 0.79, respectively, demonstrating the reduction of GO via photo-assisted process. [34,35]

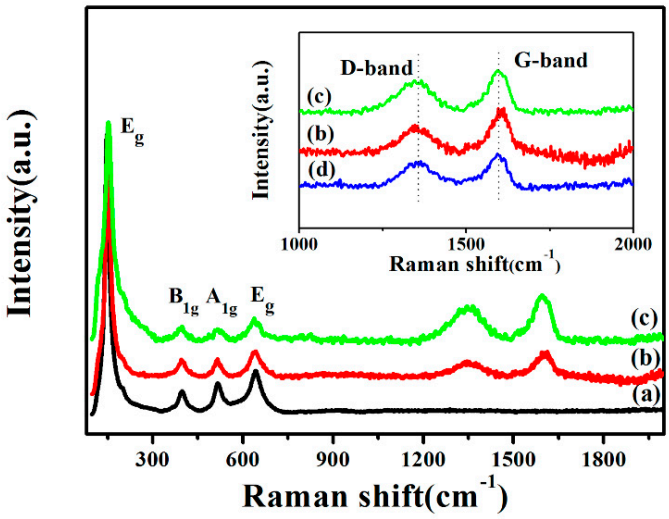

Figure 2. Raman spectra of (a) MT, (b) MTG, (c) MTGA and (d) GO (inset).

The pore structure and BET surface area of MT, MTG and MTGA nanocomposites was evaluated by the nitrogen adsorption–desorption curves shown in Figure 3. All the isotherms belong to type IV with H2 hysteresis loop, which verify that pore structure is made up of ink-bottle pores.[35] MTGA ternary nanocomposite has the large specific surface area and suitable pore size, which are investigated respectively to be 119 $m^2 g^{-1}$ and 6.55 nm, shown in Table S1. In a sense, the pore structure and large surface area would become principal factors for heightening the photocatalytic performance of MTGA nanocomposite.

Preprints (www.preprints.org) | NOT PEER-REVIEWED | Posted: 27 March 2017 doi:10.20944/preprints201703.0201.v1

Peer-reviewed version available at Catalysts 2017, 7, , 156; doi:10.3390/catal7050156

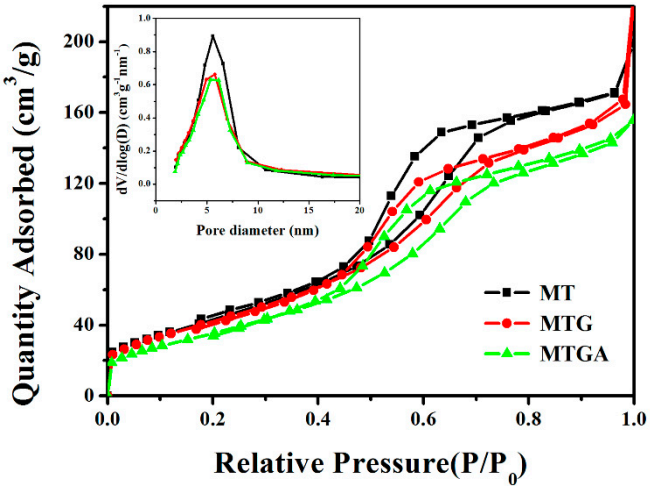

Figure 3. Nitrogen sorption isotherms and the corresponding pore size distribution curves for MT, MTG and MTGA.

The surface elemental compositions and chemical states were inspected by XPS. Figure 4 shows the existence of the elements Ti, Ag, O and C in MTGA ternary nanocomposite. In particular, as shown in Figure 4a, Ti 2p exhibits two typical peaks situated in 459.2 and 464.9 eV, noting the state of Ti^{4+} in anatase-phase TiO_2.[36] In Fig. 4b, the two peaks at 368.35 eV and 374.1 eV for Ag 3d5/2 and Ag 3d3/2 can be assigned to metallic silver (Ag^0).[37] The XPS spectrum of O 1s is divided into three peaks (532.25, 533.65 and 535.25 eV) attributing to Ti-O bond in TiO_2 nanocrystal, the Ti-OH group on the surface of TiO_2 and the –COOH species from CO_2 adsorption, respectively.[38] Moreover, the fact that GO was reduced to RGO is proved by the Figure 4d-f. The XPS spectrum in Figure 4d highlights the abundance of diverse oxygen-containing functional groups, mainly including C–OH, C–O and O=C–O on the GO surface, corresponding to the peaks position at 286, 287.4 and 289 eV.[39] It is remarkable that the attenuation of the oxygen-containing functional groups in Figure 4e and 4f of MTG and MTGA nanocomposites, which certified the reduction of GO after light illumination.[40-42]

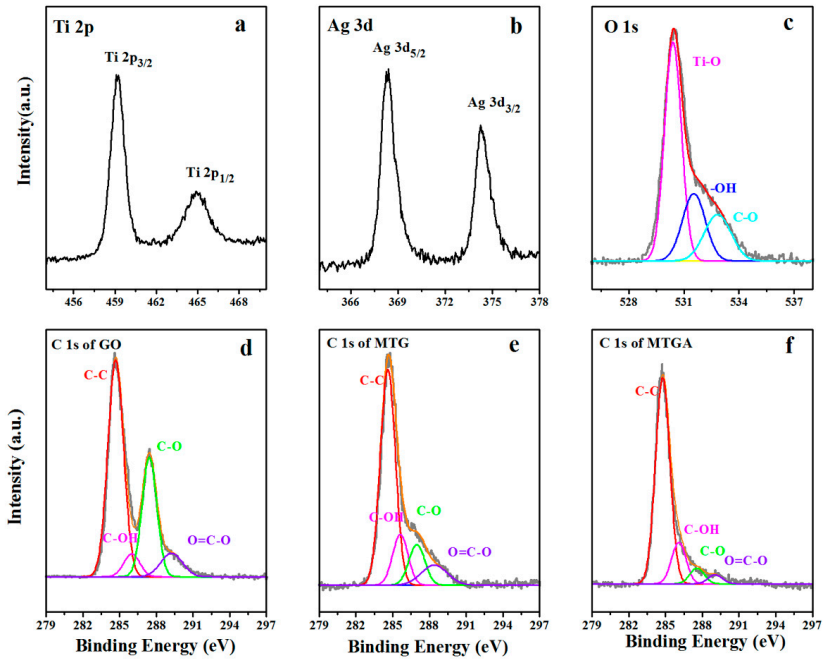

Figure 4. XPS spectra of Ti 2p (a), Ag 3d (b) and O 1s (c) of MTGA nanocomposite; XPS spectra of C 1s for GO(d), MTG (e), and MTGA (f).

Peer-reviewed version available at Catalysts 2017, 7, , 156; doi:10.3390/catal7050156

The morphology of MTGA nanocomposite can be characterized by FESEM and TEM. From the SEM image of Figure 5a, we can see that MT is agglomerating into block and its edges are encased by RGO nanosheets and Ag nanoparticles uniformly distribute on the surface of MT. The fact is also seen from Figure 5b, MT nanocrystal modified by the Ag nanoparticles adhere to the chiffon-like RGO nanosheets. The HRTEM image in Figure 5c unequivocally reveals that the specific interplanar spacings are 0.35 nm and 0.24 nm, respectively, belonging to the (101) facet of anatase TiO_2 and the (111) plane of a cubic phase Ag, which prove the coexistence of TiO_2 and Ag. Furthermore, Figure 6a-d displays the elemental mapping images based the selected area (Figure S2.) on behalf of the Ti, O, C and Ag elements, it is another-side evidence that Ag nanoparticles are deposited successfully by photo-assisted process.

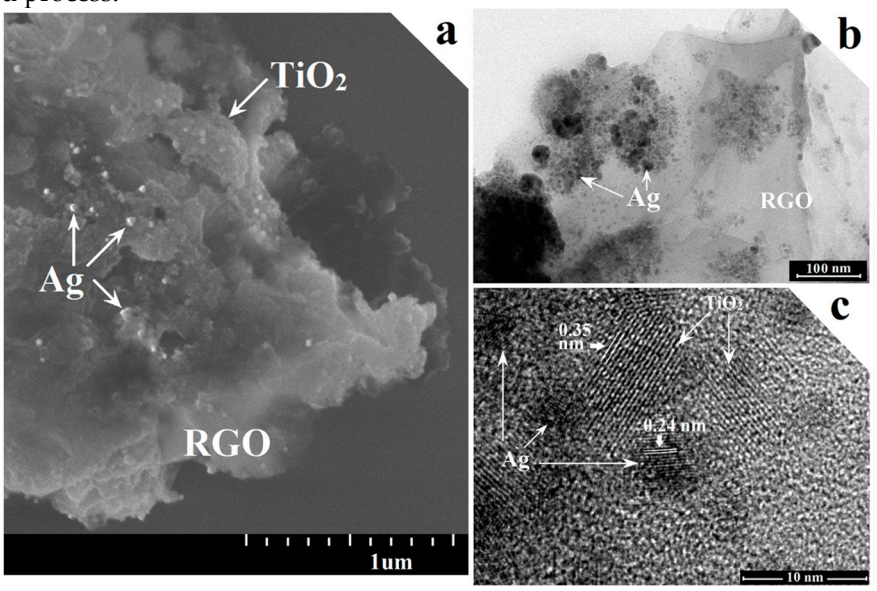

Figure 5. FESEM(a), TEM(b) and HRTEM (c) images of MTGA nanocomposite.

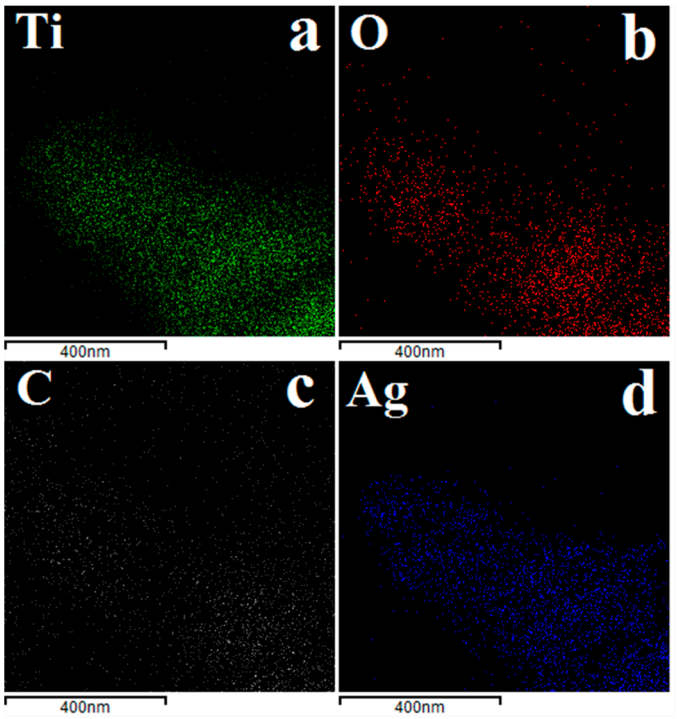

Figure 6. The corresponding elemental mapping images of Ti (a), O (b), C (c) and Ag (d).

UV-vis DRS measurements were performed to study the optical properties of the samples. As shown in Figure 7a, the pronounced absorption peak between 200 to 400 nm for all the samples is ascribed to the electron excitation from the valence band to the conduction band of TiO2. [37] In comparison, the MTG nanocomposite exhibits a broadened but weak absorbance within the visible-light region from 400 to 500 nm, which may come from the band-edge absorption of graphene. Notably, The absorption edge of MTGA exhibits an obvious red shift and the absorption range is extended to the visible-light district because of the LSPR effect of Ag nanoparticles.[20] Moreover, a plot obtained via the conversion in view of the Kubelka–Munk function versus the energy of light is shown in Figure 7b, from which the band gap energy (Eg) of MT, MTG and MTGA nanocomposites are roughly estimated to be about 3.16 eV, 2.8 eV and 2.51 eV, respectively. This suggests that the decoration of Ag nanoparticles and RGO components with the TiO_2 have a significant impact on the absorption of visible light.

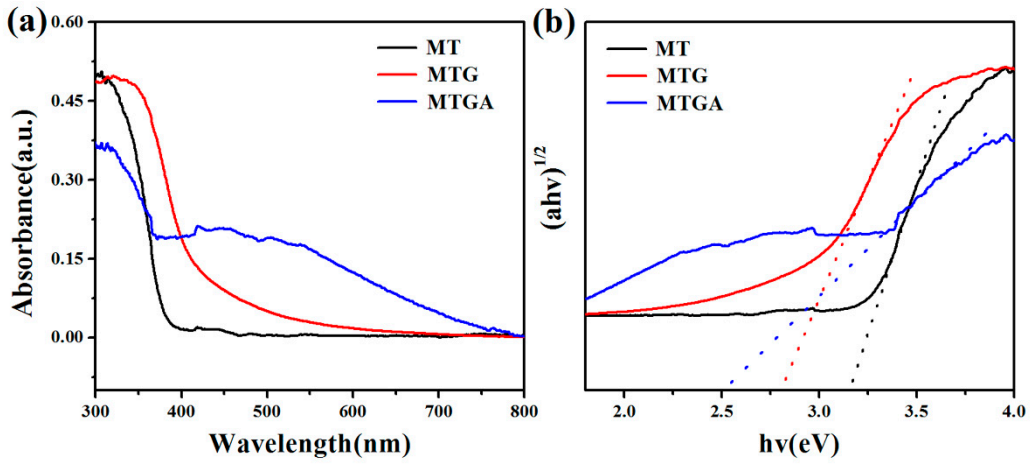

Figure 7. UV-vis DRS (a) and a plot of transformed Kubelka–Munk function versus energy of light (b) for MT, MTG and MTGA.

The photocatalytic performance of MT, MTG and MTGA was detected by the decomposition of MB dyes. As shown in Figure 8a, in the dark adsorption 30 min phase, with the increasing of silver content, the adsorption quantity is increasing until the amount reach to 8%. Following, under the condition of visible light, MB dye has the self-degradation. Excluding the self-degradation, MT basically has no the ability of degradation. Nevertheless, by contrast, MTG has a heightened photocatalytic activity to a certain extent and MTGA presents the prominently highest photocatalytic activity, whereby when the illumination time is 120 min, the degradation rate of MTGA-8 reaches 93% and the apparent reaction rate constant of the ternary material in Figure 8b is 0.017 min^{-1}, which is almost 3.4 times the degradation rate of MTG, when silver content is added up to 10%, the degradation rate does not rise rather reduced for that too much deposition of Ag nanoparticles themselves can become the recombination center that suppressing the carrier separation.[43] The stability of MTGA-8 is exhibited in Figure 9, after three cycle times, the degradation rate reduce to 91.2%. The result indicates MTGA exhibits an excellent photocatalytic capacity and the highest stability. It is facile to infer that the introduction of graphene and the loading of Ag nanoparticles can take effect together in photocatalytic activity under visible light, and that is why the ternary MTGA catalyst shows the best performance.

Preprints (www.preprints.org) | NOT PEER-REVIEWED | Posted: 27 March 2017 doi:10.20944/preprints201703.0201.v1

Peer-reviewed version available at Catalysts 2017, 7, , 156; doi:10.3390/catal7050156

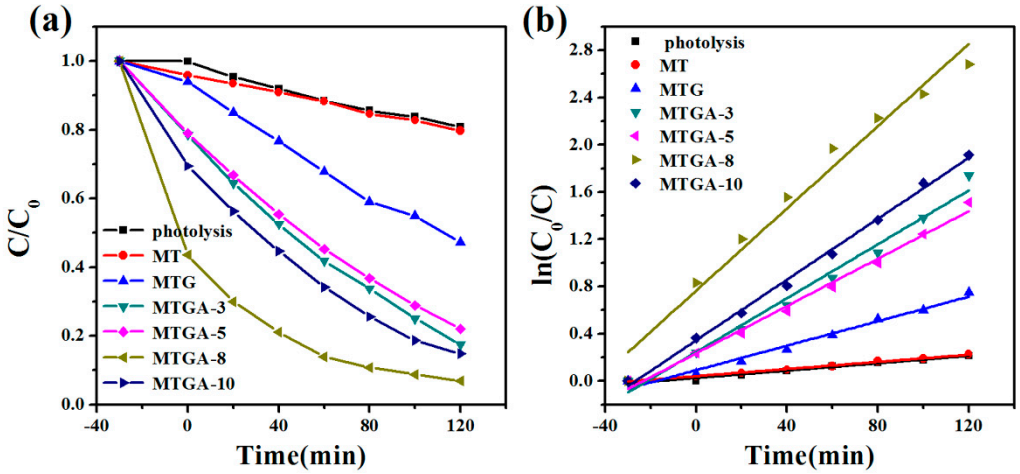

Figure 8. Photodegradation of MB (a) and the apparent reaction rate constants k (b) in the presence of visible light of MT, MTG and MTGA (with different Ag loading values)

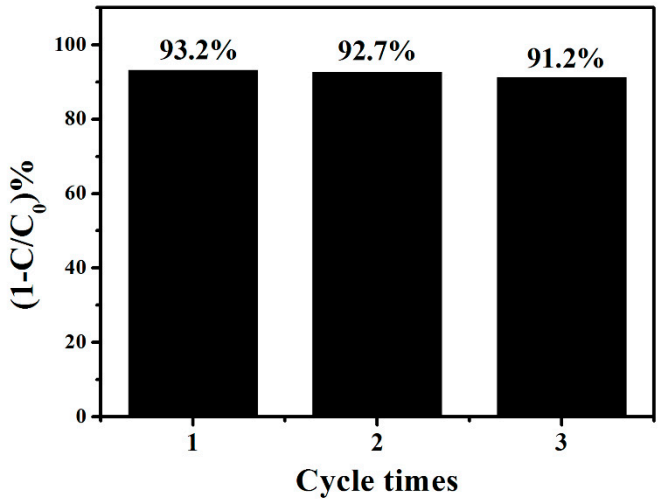

Figure 9. The cycle time of MTGA for degrading MB under visible light.

In consideration of the above results, the reason can attribute the boosted photocatalytic performance of MTGA ternary nanocomposite in the MB's decomposition to the following factors: firstly, the decoration of Ag nanoparticles can form the LSPR effect to enhance the absorbance of the TiO_2 to visible light and offer a large number of electrons scattering to CB of MT; Secondly, TiO_2 with mesoporous structure possess the large specific surface area increasing the adsorption of dyes; For another, RGO nanosheets serve as the electron acceptor that effectively accelerate the separation efficiency of carriers and provide more active sites for the degradation reaction;[44] there is potential and inseparable synergistic effect among MT, RGO and Ag that can facilitate the charge transfer and separation in MTGA nanocomposite.

Based on the above analyses, a feasible photocatalytic mechanism over MTGA ternary nanocomposite was proposed as depicted in Figure 10. Under irradiation with visible light, Ag nanoparticles can work as an electron emitter to send out electrons (e^-) to the CB of MT. Immediately, the electrons transfer from the CB of TiO_2 to RGO nanosheets owing to the favorable energy level between the CB of the TiO_2 and the work function of RGO (0.08 V vs. NHE for Fermi level),[45] in which RGO serves as a electron collector and transporter. Therefore, the path of electron transfer among Ag nanoparticles, MT and RGO is constructed to play their synergies that can effectively suppress the recombination of photogenerated electron–hole pairs. In the redox reaction, the separated electrons reduce the oxygen dissolved in the reaction system to produce O_2^- as an active

Peer-reviewed version available at Catalysts 2017, 7, , 156; doi:10.3390/catal7050156

species, which concurrently contribute to the degradation of the dye pollutant. Without ignorance, the synergistic interaction among MT, RGO and Ag nanoparticles can also play an indispensable role, therefore resulting in the significantly enhanced photoactivity of the MTGA ternary nanocomposite under visible light.

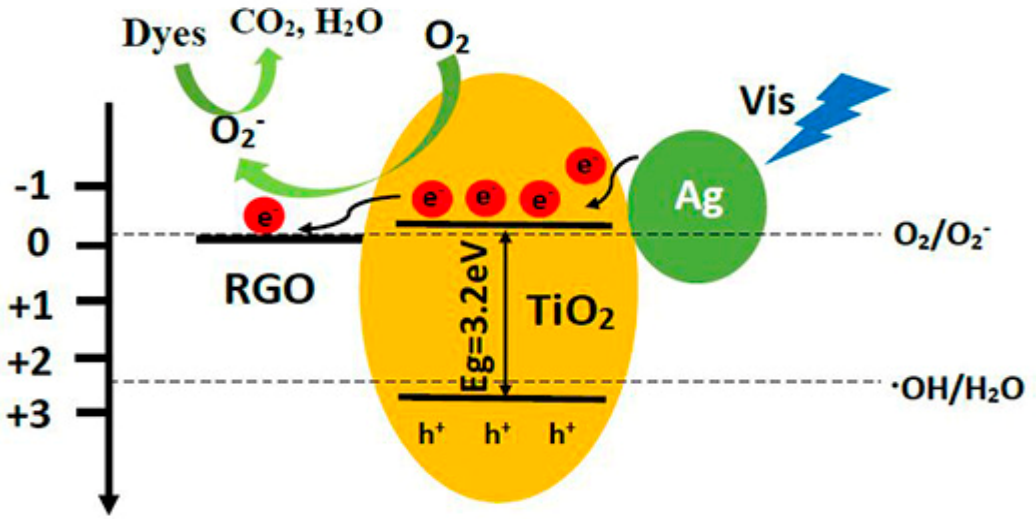

Figure. 10 Proposed mechanism diagram illustrating the photocatalytic redox reactions with the ternary MTGA catalyst in the presence of visible light.

3. Materials and Methods

2.1 Material

Pluronic@F-127 (EO96PO70EO96, MW=12 000 g/mol) was purchased from Sigma-Aldrich (USA). Tetrabutyl titanate ($Ti(OBu)_4$), acetic acid ($C_2H_4O_2$), hydrogen peroxide (H_2O_2, 30%), Silver nitrate ($AgNO_3$) and 3-aminopropyl-trimethoxysilane (APTES) were supplied by Sinopharm (Shanghai, China). Nitric acid (HNO_3), sulfuric acid (H_2SO_4), hydrochloric acid (HCl) and ethanol (C_2H_6O) were obtained from Beijing Chemical Works (Beijing, China). Graphite powder was provided from Alfa Aesar China (Tianjin, China). All the materials were used without further purification. The deionized (DI) water used in these experiments was obtained from local sources.

2.2 Synthesis

2.2.1 Synthesis of GO.

GO was produced from natural graphite fakes by a modified Hummers method.[46-48] In a typical experiment, 1 g graphite powder and 1 g $NaNO_3$ were added to 33 mL concentrated H_2SO_4 in a 3 °C ice-bath. Then, 6 g ground $KMnO_4$ was slowly added while stirring. Then, the mixture was stirred for 1.5 h at 35 °C, with slowly adding 40 mL distilled water to the mixture. The obtained mixture was stirred for a further 35 min at 90 °C. In the end, 100 mL distilled water was added to the mixture and 30 wt% H_2O_2 dropped gradually into it until the mixture turned bright yellow. Then, the mixture was washed with 150 mL 5% aqueous HCl to get rid of the metal ions, followed by washing with distilled water to effectively remove any remaining metal ions and acids. Finally, the resultant mixture was put into a vacuum drying oven at 60 °C. After 24 h, the brown exfoliated graphite oxide was obtained.

2.2.2 Synthesis of MT.

MT was obtained via the template method based on Fan's work with modifications.[49] In a typical sol–gel process, 1.6 g of F127 was dissolved in 30 mL of ethanol by stirring for 30 min, and

then stepwise was added 2.3 mL HOAc, 1.8 mL HNO_3 and 3.4 mL TBOT. The mixed solution was stirred continuously for 1 h and then poured into a 120 mm Petri dish. Then, the Petri dish was placed in an oven at 40 °C for 12 h to form a transparent membrane, followed by ageing at 65 °C for 24 h. Finally, the as prepared membranes were calcined at 350 °C in an air atmosphere for 5 h (heating rate 2 °C min^{-1}) to eventually obtain MT.

2.2.3 Synthesis of MTG and MTGA nanocomposites.

The MTGA nanocomposites was prepared by a photo-assisted reduction method.[27,46] Typically, 0.1 g MT was dispersed into 20 mL ethanol. Then, 1mL of 3-aminopropyl-trimethoxysilane (APTES) was added, and the suspension was refluxed at 80 °C for 4 h. Subsequently, the suspension was washing three times with ethanol. Afterwards, the APTES-modified MT was added into 5.26 mg GO suspension after ultrasonication with stirring for 30 min to obtain a meso-TiO_2/GO suspension. The as-obtained meso-TiO_2/GO suspension and $AgNO_3$ were dispersed in ethanol and transferred to a glass reactor. Subsequently, the glass reactor containing the suspension kept at room temperature was exposed to the simulated solar light for 2h. And then, the suspension was rinsed with ethanol and water a few times. Finally, the resultant was dried at 60 °C overnight. Similarly, MTG was synthesized by a photo-reduction in which meso-TiO_2/GO suspension was dispersed in ethanol and the above steps were repeated. Finally, we obtained the MTG and MTGA-x (x=3, 5, 8 and 10), where x indicates the mass ratio of Ag loaded onto MT.

2.3 Characterization

The as-obtained catalysts were examined with an X-ray diffractometer (XRD, a Bruker D8) with Cu Kα radiation and the Laser Confocal Micro-Raman spectroscopy with an excitation wavelength of 532 nm. X-ray photoelectron spectroscopy (XPS) measurements were conducted on a Thermo ESCALAB 250 spectrometer with a hemisphere detector at an energy resolution of 0.1 eV offered by an Al Kα radiation source. Field emission scanning electron microscope (FESEM) images were obtained by Hitchi SU8010. Transmission electron microscopy (TEM) and high-resolution transmission electron microscopy (HRTEM) images were obtained by a JEOL model JEM-2100F instrument operated at 200 kV. The Brunauer– Emmett–Teller (BET) specific surface areas of the sample powders were obtained through nitrogen adsorption–desorption, measured on JW-BK132F. Ultraviolet-visible (UV-vis) absorption spectra were surveyed using a UV-vis spectrometer (UV-2500, Shimadzu, Japan), in which BaSO4 was chosen as the reference standard.

2.4 Photocatalytic Activity

The photocatalytic degradation reaction is based on a semiconductor photocatalyst that oxidizes the target contaminants to convert to H_2O and CO_2 under visible light irradiation. In this experiment, a amount of photocatalyst was added to 10 mg/L MB solution under normal temperature and pressure. After a few minutes, the dark reaction was carried out for 30 min to allow the photocatalyst to reach the desorption equilibrium and then transferred to the photocatalytic reaction device.

Open the light source (xenon lamp 300W), take 4ml degradation solution every 20 minutes, centrifuge at 5000 r/min speed for 5-10min, the supernatant was placed in a quartz cuvette, the use of UV-vis spectrophotometer scanned in the wavelength range of 300 to 800 nm to determine the absorbance of the indicator solution after degradation. MB solution is at 664nm to reach the maximum absorbance. The absorbance of the indicator solution will change after degradation, and the change of the concentration can be calculated by absorbance rate. The photocatalytic efficiency of the photocatalyst to the indicator solution is deduced.

4. Conclusion

The ternary nanocomposite of mesoporous TiO_2/RGO/Ag has been successfully synthesized by an electrostatic self-assembly approach and a photo-assisted reduction process. Moreover, the ternary MTGA exhibited superior photocatalytic activity, for the degradation of MB under visible

light, the degradation rate reached up to 0.017 min^{-1}, which was 3.4 times than that of MTG. It is worth noting that the possible electron transfer route is that Ag nanoparticles work as an electron emitter to send out the electrons to the CB of MT, following RGO nanosheets can receive electrons to effectively separate electrons and holes. And the enhanced photocatalytic activity depends on the synergistic effect among the individual constituents of the catalyst. Therefore, the MTGA ternary nanocomposite is potentially useful for a catalyst towards photodegradation organic pollutants.

Supplementary Materials: The following are available online at www.mdpi.com/link, Table S1: Textural properties of MT, MTG and MTGA-8 nanocomposites, Figure S1: XPS survey spectrum of MTGA-8 nanocomposite, Figure S2: The selected pattern with the elemental mapping of MTGA-8 nanocomposite, Table S2: The apparent reaction rate constants k in the presence of visible light of MT, MTG and MTGA nanocomposites.

Acknowledgements: This work was supported by National Natural Science Foundation of China (51472106).

Author Contributions: C.W., H.T. and X.W. conceived and designed the experiments, collected the data; X.X. and X.H., analyzed the data and discussed the results. C.W. and H.T. wrote the paper. All authors discussed the results and commented on the manuscript.

Conflicts of Interest: The authors declare no conflict of interest.

References

1. Kumar, S.G.; Devi, L.G. Review on modified tio2 photocatalysis under uv/visible light: Selected results and related mechanisms on interfacial charge carrier transfer dynamics. *Journal Of Physical Chemistry A* **2011**, *115*, 13211-13241.
2. Hu, X.L.; Li, G.S.; Yu, J.C. Design, fabrication, and modification of nanostructured semiconductor materials for environmental and energy applications. *Langmuir* **2010**, *26*, 3031-3039.
3. Liu, S.W.; Yu, J.G.; Cheng, B.; Jaroniec, M. Fluorinated semiconductor photocatalysts: Tunable synthesis and unique properties. *Advances In Colloid And Interface Science* **2012**, *173*, 35-53.
4. Liu, G.; Wang, L.Z.; Yang, H.G.; Cheng, H.M.; Lu, G.Q. Titania-based photocatalysts-crystal growth, doping and heterostructuring. *Journal Of Materials Chemistry* **2010**, *20*, 831-843.
5. Yang, H.G.; Sun, C.H.; Qiao, S.Z.; Zou, J.; Liu, G.; Smith, S.C.; Cheng, H.M.; Lu, G.Q. Anatase tio2 single crystals with a large percentage of reactive facets. *Nature* **2008**, *453*, 638-U634.
6. Dozzi, M.V.; Selli, E. Specific facets-dominated anatase tio2: Fluorine-mediated synthesis and photoactivity. *Catalysts* **2013**, *3*, 455-485.
7. Yu, Y.; Yu, J.C.; Yu, J.G.; Kwok, Y.C.; Che, Y.K.; Zhao, J.C.; Ding, L.; Ge, W.K.; Wong, P.K. Enhancement of photocatalytic activity of mesoporous tio2 by using carbon nanotubes. *Applied Catalysis a-General* **2005**, *289*, 186-196.
8. Yu, J.G.; Ma, T.T.; Liu, S.W. Enhanced photocatalytic activity of mesoporous tio2 aggregates by embedding carbon nanotubes as electron-transfer channel. *Physical Chemistry Chemical Physics* **2011**, *13*, 3491-3501.
9. Williams, G.; Seger, B.; Kamat, P.V. Tio2-graphene nanocomposites. Uv-assisted photocatalytic reduction of graphene oxide. *Acs Nano* **2008**, *2*, 1487-1491.
10. Li, G.S.; Zhang, D.Q.; Yu, J.C. A new visible-light photocatalyst: Cds quantum dots embedded mesoporous tio2. *Environmental Science & Technology* **2009**, *43*, 7079-7085.
11. Ge, M.Z.; Cao, C.Y.; Li, S.H.; Tang, Y.X.; Wang, L.N.; Qi, N.; Huang, J.Y.; Zhang, K.Q.; Al-Deyab, S.S.; Lai, Y.K. In situ plasmonic ag nanoparticle anchored tio2 nanotube arrays as visible-light-driven photocatalysts for enhanced water splitting. *Nanoscale* **2016**, *8*, 5226-5234.
12. Tian, H.; Shen, K.; Hu, X.; Qiao, L.; Zheng, W. N, s co-doped graphene quantum dots-graphene-tio2 nanotubes composite with enhanced photocatalytic activity. *Journal of Alloys and Compounds* **2017**, *691*, 369-377.
13. Xie, C.; Yang, S.H.; Shi, J.W.; Niu, C.M. Highly crystallized c-doped mesoporous anatase tio2 with visible light photocatalytic activity. *Catalysts* **2016**, *6*.

14. Eda, G.; Fanchini, G.; Chhowalla, M. Large-area ultrathin films of reduced graphene oxide as a transparent and flexible electronic material. *Nature Nanotechnology* **2008**, *3*, 270-274.
15. Stankovich, S.; Dikin, D.A.; Dommett, G.H.B.; Kohlhaas, K.M.; Zimney, E.J.; Stach, E.A.; Piner, R.D.; Nguyen, S.T.; Ruoff, R.S. Graphene-based composite materials. *Nature* **2006**, *442*, 282-286.
16. Xiang, Q.; Yu, J.; Jaroniec, M. Graphene-based semiconductor photocatalysts. *Chemical Society Reviews* **2012**, *41*, 782-796.
17. Wang, W.G.; Yu, J.G.; Xiang, Q.J.; Cheng, B. Enhanced photocatalytic activity of hierarchical macro/mesoporous tio2-graphene composites for photodegradation of acetone in air. *Applied Catalysis B-Environmental* **2012**, *119*, 109-116.
18. Zhang, H.; Lv, X.J.; Li, Y.M.; Wang, Y.; Li, J.H. P25-graphene composite as a high performance photocatalyst. *Acs Nano* **2010**, *4*, 380-386.
19. Liu, J.C.; Bai, H.W.; Wang, Y.J.; Liu, Z.Y.; Zhang, X.W.; Sun, D.D. Self-assembling tio2 nanorods on large graphene oxide sheets at a two-phase interface and their anti-recombination in photocatalytic applications. *Advanced Functional Materials* **2010**, *20*, 4175-4181.
20. He, X.L.; Cai, Y.Y.; Zhang, H.M.; Liang, C.H. Photocatalytic degradation of organic pollutants with ag decorated free-standing tio2 nanotube arrays and interface electrochemical response. *Journal of Materials Chemistry* **2011**, *21*, 475-480.
21. Ismail, A.A. Facile synthesis of mesoporous ag-loaded tio2 thin film and its photocatalytic properties. *Microporous and Mesoporous Materials* **2012**, *149*, 69-75.
22. Sellappan, R.; Nielsen, M.G.; Gonzalez Posada, F.; Vesborg, P.C.K.; Chorkendorff, I.; Chakarov, D. Effects of plasmon excitation on photocatalytic activity of ag/tio2 and au/tio2 nanocomposites. *Journal of Catalysis* **2013**, *307*, 214-221.
23. Sher Shah, M.S.; Zhang, K.; Park, A.R.; Kim, K.S.; Park, N.G.; Park, J.H.; Yoo, P.J. Single-step solvothermal synthesis of mesoporous ag-tio2-reduced graphene oxide ternary composites with enhanced photocatalytic activity. *Nanoscale* **2013**, *5*, 5093-5101.
24. Kumar, R.; El-Shishtawy, R.M.; Barakat, M.A. Synthesis and characterization of ag-ag2o/tio2@polypyrrole heterojunction for enhanced photocatalytic degradation of methylene blue. *Catalysts* **2016**, *6*.
25. Xian, J.J.; Li, D.Z.; Chen, J.; Li, X.F.; He, M.; Shao, Y.; Yu, L.H.; Fang, J.L. Tio2 nanotube array-graphene-cds quantum dots composite film in z-scheme with enhanced photoactivity and photostability. *Acs Applied Materials & Interfaces* **2014**, *6*, 13157-13166.
26. Myilsamy, M.; Murugesan, V.; Mahalakshmi, M. Indium and cerium co-doped mesoporous tio2 nanocomposites with enhanced visible light photocatalytic activity. *Applied Catalysis a-General* **2015**, *492*, 212-222.
27. Li, W.Q.; Liu, X.; Li, H.X. Hydrothermal synthesis of graphene/fe3+-doped tio2 nanowire composites with highly enhanced photocatalytic activity under visible light irradiation. *Journal of Materials Chemistry A* **2015**, *3*, 15214-15224.
28. Lin, X.; Xu, D.; Lin, Z.; Jiang, S.S.; Chang, L.M. Construction of heterostructured tio2/invo4/rgo microspheres with dual-channels for photo-generated charge separation. *Rsc Advances* **2015**, *5*, 84372-84380.
29. Li, L.; Wu, B.H.; Li, G.N.; Li, Y.S. C, n co-doping promoted mesoporous au/tio2 catalyst for low temperature co oxidation. *Rsc Advances* **2016**, *6*, 28904-28911.
30. Xue, C.; Yan, X.; Ding, S.; Yang, G. Monodisperse ag–agbr nanocrystals anchored on one-dimensional tio2 nanotubes with efficient plasmon-assisted photocatalytic performance. *RSC Advances* **2016**, *6*.
31. Vasilaki, E.; Georgaki, I.; Vernardou, D.; Vamvakaki, M.; Katsarakis, N. Ag-loaded tio2/reduced graphene oxide nanocomposites for enhanced visible-light photocatalytic activity. *Applied Surface Science* **2015**, *353*, 865-872.
32. Tan, L.-L.; Ong, W.-J.; Chai, S.-P.; Mohamed, A.R. Noble metal modified reduced graphene oxide/tio2 ternary nanostructures for efficient visible-light-driven photoreduction of carbon dioxide into methane. *Applied Catalysis B: Environmental* **2015**, *166-167*, 251-259.

33. Leong, K.H.; Sim, L.C.; Bahnemann, D.; Jang, M.; Ibrahim, S.; Saravanan, P. Reduced graphene oxide and ag wrapped tio2 photocatalyst for enhanced visible light photocatalysis. *APL Materials* **2015**, *3*, 104503.
34. Tian, H.; Wan, C.; Zheng, W.; Hu, X.; Qiao, L.; Wang, X. Construction of a ternary hybrid of cds nanoparticles loaded on mesoporous-tio2/rgo for the enhancement of photocatalytic activity. *RSC Adv.* **2016**, *6*, 84722-84729.
35. Liu, S.W.; Liu, C.; Wang, W.G.; Cheng, B.; Yu, J.G. Unique photocatalytic oxidation reactivity and selectivity of tio2-graphene nanocomposites. *Nanoscale* **2012**, *4*, 3193-3200.
36. Xiao, F. An efficient layer-by-layer self-assembly of metal-tio2 nanoring/nanotube heterostructures, m/t-nrnt (m = au, ag, pt), for versatile catalytic applications. *Chemical Communications* **2012**, *48*, 6538-6540.
37. Xiao, F. Layer-by-layer self-assembly construction of highly ordered metal-tio2 nanotube arrays heterostructures (m/tnts, m = au, ag, pt) with tunable catalytic activities. *Journal of Physical Chemistry C* **2012**, *116*, 16487-16498.
38. Xiao, F.X.; Miao, J.; Liu, B. Self-assembly of aligned rutile@anatase tio2 nanorod@cds quantum dots ternary core-shell heterostructure: Cascade electron transfer by interfacial design. *Materials Horizons* **2014**, *1*, 259-263.
39. Benedetti, J.E.; Bernardo, D.R.; Morais, A.; Bettini, J.; Nogueira, A.F. Synthesis and characterization of a quaternary nanocomposite based on tio2/cds/rgo/pt and its application in the photoreduction of co2 to methane under visible light. *Rsc Advances* **2015**, *5*, 33914-33922.
40. Pan, X.Y.; Xu, Y.J. Graphene-templated bottom-up fabrication of ultralarge binary cds-tio2 nanosheets for photocatalytic selective reduction. *Journal of Physical Chemistry C* **2015**, *119*, 7184-7194.
41. Zhang, Y.H.; Tang, Z.R.; Fu, X.; Xu, Y.J. Engineering the unique 2d mat of graphene to achieve graphene-tio2 nanocomposite for photocatalytic selective transformation: What advantage does graphene have over its forebear carbon nanotube? *Acs Nano* **2011**, *5*, 7426-7435.
42. Zhang, Y.H.; Zhang, N.; Tang, Z.R.; Xu, Y.J. Graphene transforms wide band gap zns to a visible light photocatalyst. The new role of graphene as a macromolecular photosensitizer. *Acs Nano* **2012**, *6*, 9777-9789.
43. Grabowska, E.; Zaleska, A.; Sorgues, S.; Kunst, M.; Etcheberry, A.; Colbeaujustin, C.; Remita, H. Modification of titanium(iv) dioxide with small silver nanoparticles: Application in photocatalysis. *Journal of Physical Chemistry C* **2013**, *117*, 1955–1962.
44. Fan, W.Q.; Yu, X.Q.; Lu, H.C.; Bai, H.Y.; Zhang, C.; Shi, W.D. Fabrication of tio2/rgo/cu2o heterostructure for photoelectrochemical hydrogen production. *Applied Catalysis B-Environmental* **2016**, *181*, 7-15.
45. Wang, X.W.; Tian, H.W.; Cui, X.Q.; Zheng, W.T.; Liu, Y.C. One-pot hydrothermal synthesis of mesoporous $zn_xcd_{1-x}s$/reduced graphene oxide hybrid material and its enhanced photocatalytic activity. *Dalton Transactions* **2014**, *43*, 12894-12903.
46. Stankovich, S.; Dikin, D.A.; Piner, R.D.; Kohlhaas, K.A.; Kleinhammes, A.; Jia, Y.; Wu, Y.; Nguyen, S.T.; Ruoff, R.S. Synthesis of graphene-based nanosheets via chemical reduction of exfoliated graphite oxide. *Carbon* **2007**, *45*, 1558-1565.
47. Park, S.; Ruoff, R.S. Chemical methods for the production of graphenes. *Nature Nanotechnology* **2009**, *4*, 217-224.
48. Zhu, Y.; Murali, S.; Cai, W.; Li, X.; Suk, J.W.; Potts, J.R.; Ruoff, R.S. Graphene and graphene oxide: Synthesis, properties, and applications. *Advanced Materials* **2010**, *22*, 3906-3924.
49. Fan, J.; Boettcher, S.W.; Stucky, G.D. Nanoparticle assembly of ordered multicomponent mesostructured metal oxides via a versatile sol-gel process. *Chemistry Of Materials* **2006**, *18*, 6391-6396.